BIOCHEMISTRY
including biophysical chemistry & molecular biology

ARTICLE

pubs.acs.org/biochemistry

Role of Packing Defects in the Evolution of Allostery and Induced Fit in Human UDP-Glucose Dehydrogenase

Renuka Kadirvelraj,[†] Nicholas C. Sennett,[†] Samuel J. Polizzi,[†] Stephen Weitzel,[‡] and Zachary A. Wood*[,†]

[†]Department of Biochemistry and Molecular Biology, University of Georgia, Athens, Georgia 30602, United States

[‡]Institute of Molecular Biology, University of Oregon, Eugene, Oregon 97403, United States

Supporting Information

ABSTRACT: Allosteric feedback inhibition is the mechanism by which metabolic end products regulate their own biosynthesis by binding to an upstream enzyme. Despite its importance in controlling metabolism, there are relatively few allosteric mechanisms understood in detail. This is because allostery does not have an identifiable structural motif, making the discovery of new allosteric enzymes a difficult process. The lack of a conserved motif implies that the evolution of each allosteric mechanism is unique. Here we describe an atypical allosteric mechanism in human UDP-α-D-glucose 6-dehydrogenase (hUGDH) based on an easily acquired and identifiable structural attribute: packing defects in the protein core. In contrast to classic allostery, the active and allosteric sites in hUGDH are present as a single, bifunctional site. Using two new crystal structures, we show that binding of the feedback inhibitor, UDP-α-D-xylose, elicits a distinct induced-fit response; a buried loop translates ~4 Å along and rotates ~180° about the main chain axis, requiring surrounding side chains to repack. This allosteric transition is facilitated by packing defects, which negate the steric conformational restraints normally imposed by the protein core. Sedimentation velocity studies show that this repacking favors the formation of an inactive hexameric complex with unusual symmetry. We present evidence that hUGDH and the unrelated enzyme dCTP deaminase have converged to very similar atypical allosteric mechanisms using the same adaptive strategy, the selection for packing defects. Thus, the selection for packing defects is a robust mechanism for the evolution of allostery and induced fit.

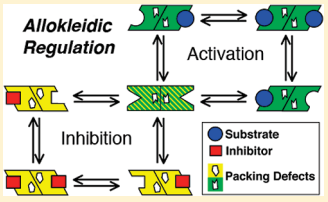

The nucleotide sugar UDP-α-D-glucuronic acid (UGA) is an essential substrate in two biochemical pathways with special relevance to cancer biology: (i) maintenance of the extracellular matrix through proteoglycan and hyaluronan biosynthesis and (ii) phase II metabolism of drugs. The first pathway controls metastasis; disrupting proteoglycan or hyaluronan biosynthesis has been shown to attenuate tumor growth and progression.[1−5] The second pathway (phase II metabolism) limits the effectiveness of chemotherapeutics by conjugating glucuronic acid to drugs. These glucuronides are rapidly eliminated from the body. In fact, some colon and lung cancers have been shown to use glucuronidation as an effective drug resistance mechanism.[6−12] Thus, understanding how UGA biosynthesis is regulated is an important goal in developing strategies to slow metastasis, alter the pharmacokinetic properties of chemotherapeutics, and sensitize tumors that use glucuronidation as a drug resistance mechanism.

Human UDP-α-D-glucose 6-dehydrogenase (hUGDH) catalyzes the NAD^+-dependent oxidation of UDP-α-D-glucose (UDG) to UGA. In addition to its roles in maintaining the extracellular matrix and drug metabolism, UGA is also the substrate for the biosynthesis of UDP-α-D-xylose (UDX) (Figure 1A). UDX is an essential nucleotide sugar in proteoglycan biosynthesis and a feedback inhibitor that controls hUGDH activity.[13,14] Even though UDX was first recognized as a feedback inhibitor of hUGDH more than 45 years ago,[13] the mechanism of inhibition was poorly understood. On the basis of the sigmoidal inhibition kinetics, it was initially believed that the feedback mechanism of hUGDH would be allosteric.[13] In later studies, Gainey et al. identified hysteresis in the kinetics of UDX binding and proposed an alternative model for the cooperativity observed in the feedback inhibition of hUGDH.[15] Hysteretic enzymes exhibit a slow conformational change between active and inactive states.[16,17] This slow transition can produce a phenomenon known as kinetic cooperativity.[16,17] Briefly, the rate at which the Michaelis complex forms depends on the concentration of substrate (k_1[E][S]) (Figure 1B). At low substrate concentrations, the slow inactivation step (k_3[E]) can compete with the slow formation of the Michaelis complex and reduce the apparent rate of the reaction. At higher substrate concentrations, the rapid formation of the Michaelis complex effectively traps the enzyme in the active state. Because the concentration of the active enzyme is increasing with substrate, the resulting substrate saturation curves will be sigmoidal because of a kinetic, not allosteric, process. Later work by Dickinson suggested that hysteresis in hUGDH was due to the slow dissociation of an inactive oligomeric complex to form the active species.[18] Thus, if UDX binding stabilizes or induces the formation of the inactive oligomer, feedback inhibition could exhibit kinetic cooperativity.

Received: April 14, 2011
Revised: May 17, 2011
Published: May 19, 2011

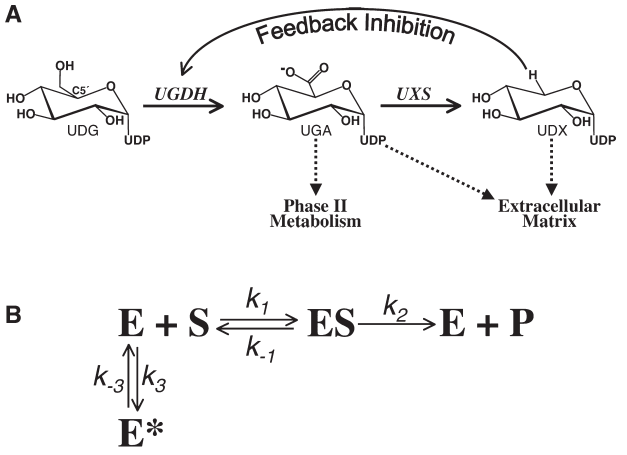

Figure 1. Regulation of UDP-glucose dehydrogenase. (A) UDP-glucose dehydrogenase (UGDH) oxidizes UDP-glucose (UDG) to UDP-glucuronic acid (UGA), which is then decarboxylated by UDP-xylose synthase (UXS) to produce the feedback inhibitor UDP-xylose (UDX). The C5′ atom of UDG is labeled. Dashed lines indicate the metabolic pathways in which UGA and UDX are essential substrates. (B) Enzyme hysteresis occurs when the transition between the inactive (E*) and active (E) forms of an enzyme is not at equilibrium with the formation and turnover of the Michaelis complex (ES).

The aim of this paper is to determine the feedback inhibition mechanism of hUGDH. Here we show that UDX inhibition of hUGDH involves an atypical form of allostery; the active and allosteric sites in hUGDH are present as a single, bifunctional site. Binding of the feedback inhibitor UDX induces a remarkable repacking of the protein core that converts the enzyme into an inactive, low-symmetry complex. We also present evidence that hUGDH and an unrelated enzyme, dCTP-deaminase, both converged to similar, atypical allosteric mechanisms by selecting for large packing defects (cavities, voids, and pockets)[19] near preexisting, smaller defects. These packing defects are key to the distinct induced-fit conformations that accommodate the binding of the substrate or the allosteric inhibitor. Thus, packing defects may represent hot spots for the evolution of allosteric networks and induced fit.

MATERIALS AND METHODS

Protein Expression and Purification. The sequence for hUGDH was synthesized (Geneart) and cloned into a pet15b plasmid vector modified to contain a tobacco etch virus (TEV) cleavage site prior to the Met start codon of the gene. Rosetta (DE3) pLysS cells containing the construct were grown at 37 °C to an OD_{600} of 0.9−1.0 (4 L) and then induced overnight at 20 °C with 0.15 mM isopropyl β-D-thiogalactoside. Cells were sonicated in 100 mL of 50 mM phosphate (pH 7.8) and 300 mM NaCl. Recombinant hUGDH was purified using Talon metal affinity resin, and the His tag was removed with codon-optimized TEV protease.[20] The purified protein was dialyzed into its storage buffer [25 mM Tris (pH 8), 50 mM NaCl, and 2 mM β-mercaptoethanol] and concentrated to 12 mg/mL.

Crystallization, Structure Solution, and Analysis. Protein containing 5 mM UDP-xylose (Carbosource, CCRC, at the University of Georgia) and either 5 mM NAD^+ (crystal form **1**) or 5 mM NADH (crystal form **2**) was used for crystallization screens. Crystals were grown at 26 °C using the hanging drop vapor diffusion method with 2 μL drops mixed in a 1:1 ratio (protein:reservoir). The reservoir contained 6% heptanediol, 10% PEG 3350, and 100 mM HEPES (pH 7.5) for hUGDH:UDX:NAD^+ crystal form **1** (monoclinic $P2_1$) or 15% hexanediol, 10% PEG 3350, and 100 mM HEPES (pH 7) for hUGDH:UDX:NADH crystal form **2** (orthorhombic $P2_12_12_1$). Crystals grew as triangular plates within ∼7−10 days from both conditions.

Crystals were cryoprotected with 20% glycerol containing the appropriate ligands at 2 mM and plunged into liquid nitrogen prior to data collection. Diffraction data were collected at beamline 22-ID (SER-CAT) at the Argonne National Laboratory using a MAR 300 mm CCD detector, a wavelength of 1 Å, and an oscillation step of 1.0° for crystal form **1** or 0.5° for crystal form **2**. Data were processed with XDS,[21] and 5% of the data were set aside for cross-validation. Crystal parameters and data collection and refinement statistics are summarized in Table 1.

The structures were determined by molecular replacement using PHASER[22] and chain A of Protein Data Bank (PDB) entry 2Q3E as a search model (bound ligands and water were removed prior to the search). Both structures (crystal forms **1** and **2**) contained a complete, broken hexamer in the asymmetric unit. Initial model refinement involved iterative cycles of manual rebuilding of the peptide using COOT[23] and refinement with REFMAC5.[24] This was followed by the location and refinement of bound ligands and ordered water molecules. Loop residues 382−388 were disordered in both structures.

Protein domain motion was analyzed using DynDom.[25] Packing defects were identified using CASTp[26] with a probe radius of 1.4 Å. All figures were generated with Pymol (http://pymol.sourceforge.net) unless otherwise specified.

Analytical Ultracentrifugation. Sedimentation velocity studies were performed using an Optima XLA analytical ultracentrifuge (Beckman Coulter). For all samples, 9.1 μM hUGDH was dialyzed into buffer [25 mM Tris (pH 8.0) and 175 mM NaCl] with or without 79 μM ligand (UDG or UDX). For analysis, samples were loaded into cells with 12 mm centerpieces and equilibrated for ∼1 h at 20 °C. Cells were loaded into an An60 Ti rotor and run at 50000 rpm. Data were collected at a wavelength of 280 nm using a radial step size of 0.003 cm. The partial specific volume of 0.7384 mL/g was calculated from the amino acid sequence. The buffer density of 1.00616 g/mL and the viscosity of 0.010253 P were calculated using SEDNTERP.[27] All data were analyzed using SEDFIT.[28] Continuous sedimentation coefficient distribution analyses were restrained by maximum entropy regularization at a P = 0.68 confidence interval. The baseline, meniscus, frictional coefficient, and systematic time-invariant and radial-invariant noise were fitted. The root-mean-square deviation (rmsd) values for all reported experiments were ≤0.009 OD.

RESULTS AND DISCUSSION

UDX Inhibition Reduces the Symmetry of the hUGDH Hexamer. We have determined the crystal structures of two different UDX-inhibited hUGDH complexes: hUGDH:UDX:NAD^+ and hUGDH:UDX:NADH (Table 1). The hUGDH:UDX:NAD^+ complex crystallized in space group $P2_1$ and was refined to 2.5 Å resolution. The hUGDH:UDX:NADH complex crystallized in higher-symmetry space group $P2_12_12_1$ but diffracted only to 3.1 Å resolution. The rmsd between the two crystal forms is 0.28 Å for 458 corresponding Cα atoms.

Table 1. Data Collection and Refinement Statistics (molecular replacement)

	crystal form **1**	crystal form **2**
	Data Collection	
Protein Data Bank entry	3PTZ	3PRJ
space group	$P2_1$	$P2_12_12_1$
unit cell dimensions (a, b, c, α, β, γ)	89.1 Å, 196.7 Å, 111.7 Å, 90.0°, 111.9°, 90.0°	111.8 Å, 160.6 Å, 205.9 Å, 90.0°, 90.0°, 90.0°
R_{meas}	9.2 (48)[a]	8.5 (42.6)[a]
$R_{mrgd\text{-}F}$	11.8 (52.2)	10.3 (44.2)
$I/\sigma I$	15.9 (3.2)	17 (3.8)
completeness (%)	96.5 (90.3)	96.9 (92.5)
redundancy	3.8 (3.4)	4.1 (3.5)
	Refinement	
resolution (Å)	2.5	3.1
no. of reflections	113593	62511
R_{work}/R_{free}	0.19/0.26	0.23/0.27
no. of atoms	22754	22213
protein	21502	21597
ligand	468	468
water	784	148
B factor		
protein	31.7	54.7
ligand	32	50.7
water	28.8	27.8
stereochemical ideality		
bond lengths (Å)	0.018	0.014
bond angles (deg)	1.7	1.4
ϕ and ψ in the most favored region (%)	88.3	88.9
ϕ and ψ in the allowed region (%)	11.6	10.9
ϕ and ψ in the generously allowed region (%)	0.1	0.2

[a] Values in parentheses are for the highest-resolution shell.

The N-terminal (residues 1−212) and C-terminal (residues 323−466) domains of hUGDH each contain a Rossmann fold for binding NAD^+ and UDG, respectively (Figure 2A). The terminal domains are connected by an α-helical domain (residues 213−322) that forms a dimer-building interface and buries ∼2600 $Å^2$ of surface per monomer. The structure of the UGDH dimer is highly conserved. Two crystal structures of *Streptococcus pyogenes* UGDH have been described in the literature:[29] *Sp*UGDH:UDX:NAD^+ and *Sp*UGDH:UGA:NADH. Despite a low level of sequence identity of 23%, the entire hUGDH and *Sp*UGDH dimers overlay with an rmsd of 1.8 Å for 732 corresponding Cα atoms (Figure 2B,C).

In addition to our new structures, the Structural Genomics Consortium (Oxford, England) has deposited four crystal structures of hUGDH: two mixed substrate−product complexes [hUGDH:UDG:NADH (PDB entry 2Q3E) and hUGDH:UGA:NAD^+ (PDB entry 2QG4)], hUGDH in complex with a covalent thioester intermediate (PDB entry 3KHU), and an apo form with an active site mutation (PDB entry 3ITK). These four hUGDH structures reveal a hexamer displaying point group symmetry 32 (or a trimer of dimers) hereafter termed the "high-symmetry hexamer" (Figure 3A). The hexamer-building interface in hUGDH is formed from a series of inserted loops not conserved in *Sp*UGDH (Figure 2). In contrast, both of our UDX-inhibited structures reveal a low-symmetry complex (point group symmetry 2) that we call the "broken hexamer" (Figure 3B). The broken-hexamer conformation is related to the high-symmetry hexamer by a 10.5° rigid-body rotation about an axis centered in the hexamer-building interface (Figure 3C). Previous studies have shown that hUGDH forms a hexamer in solution,[30] but our results suggest two distinct hexameric complexes are possible. To resolve this apparent ambiguity, we investigated the hUGDH complexes using sedimentation velocity. These studies reveal that apo-UGDH is a complex distribution in solution, consisting predominantly of hexamers and dimers, with a small amount of monomers and tetramers also present (Figure 3D). Adding 79 μM substrate UDG ($K_M \cong$ 10−20 μM[30,31]) has little or no effect on the distribution (Figure 3D). These results show that the high-symmetry hexamer is a relatively weak complex and that the high protein concentrations during crystallization stabilized the structure. In contrast, 79 μM inhibitor UDX ($K_i \cong 10\ \mu$M[13]) has a profound effect on the enzyme conformation and stabilizes a hexameric species with a sedimentation coefficient of 12.7 S (Figure 3E). This is slightly more than the *S* values of the apo and UDG-bound hexamers (11.5 S) and suggests a difference in the conformational states. Alternatively, the smaller *S* value of the apo and UDG-bound hexamers is also consistent with the existence of a rapid equilibrium with the lower-molecular weight species. Our observation of the same structure in two different space groups is strong evidence that UDX-inhibited hUGDH forms the broken-hexamer conformation in solution, based on

dx.doi.org/10.1021/bi2005637 |*Biochemistry* 2011, 50, 5780–5789

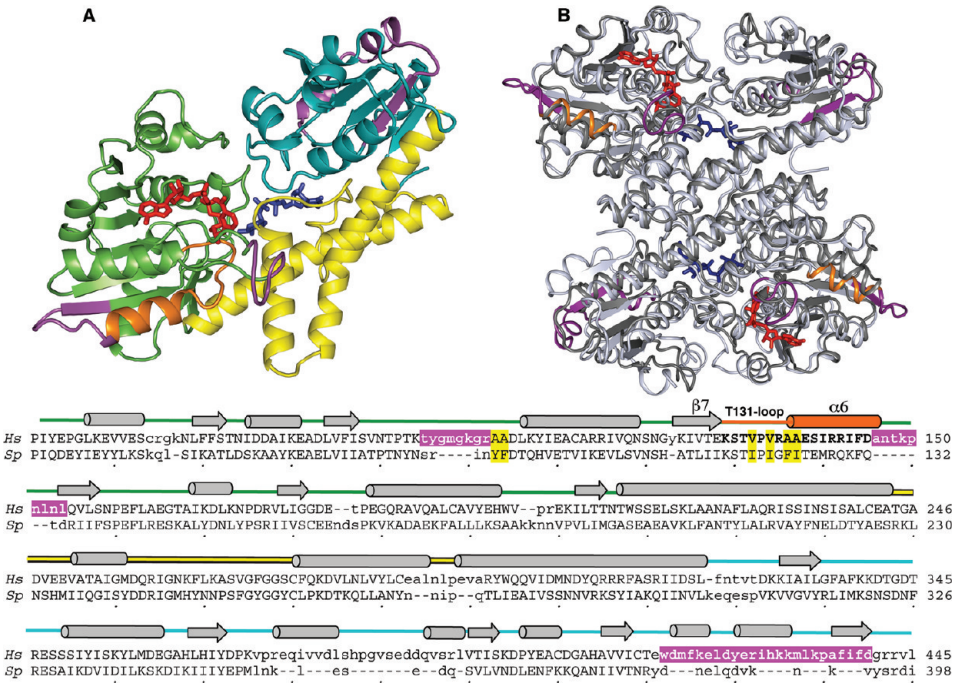

Figure 2. Human and bacterial UGDH are highly conserved. (A) Cartoon rendering of hUGDH depicting the N-terminal domain (green), the α-helical dimer interface (yellow), and the C-terminal domain (teal). Inserted elements that make up the hexamer-building interface are colored purple (see the text for details). The Thr131 loop and α6 helix are colored orange. UDX (blue) and NADH (red) are depicted as sticks. (B) Conserved structure of the UGDH dimer. The human UGDH:UDX:NAD^+ complex is colored light gray and the bacterial UGDH:UDX:NAD^+ complex (PDB entry 1DLI) dark gray. The Thr131 loop, the α6 helix, and the inserted elements in the human enzyme are colored as described for panel A. (C) Structure-based sequence alignment of human (residues 50−445) and *S. pyogenes* (residues 43−398) UGDH. α-Helices (cylinders) and β-sheets (arrows) are shown with the color of the line connecting the structural elements identifying the N-terminal (green), dimerization (yellow), and C-terminal (teal) domains. Inserted elements that make up the hexamer-building interface in hUGDH are highlighted in purple. The large-to-small amino acid substitutions surrounding the Thr131 loop in the human enzyme are highlighted in yellow (see the text for details). The Thr131 loop and α6 helix are colored orange and shown in bold letters.

the following. (i) UDX stabilizes the hexameric complex. (ii) Crystal nucleation selects for low-energy conformations.[32] (iii) Crystal lattice forces are too weak to deform a protein structure.[32,33]

The Thr131 Loop Is the Allosteric Switch That Stabilizes the Broken Hexamer. UDX lacks the C5′-hydroxymethyl found in the substrate, UDG (Figure 1A). To determine how the small difference between UDX and UDG disrupts the hexamer, we compared our structures to the 2 Å resolution high-symmetry hUGDH:UDG:NADH hexamer complex (PDB entry 2Q3E). The monomers of the high-symmetry and broken-hexamer complexes superimpose with an rmsd of 0.7 Å for 456 corresponding Cα atoms. In the high-symmetry hexamer, the NAD cofactor and UDG substrate bind in extended conformations in the active site, positioning the nicotinamide and the pyranose at the junction of the two terminal domains (Figure 2A). The active site structure is conserved with *Sp*UGDH, which has already been described in detail.[29] Specifically, the C5′-hydroxymethyl (C6′-OH) makes hydrogen bonds with Asn224 and the catalytic base Lys220 and places the C6′ atom of UDG within ∼3.4 Å of S_γ of Cys276, the active site nucleophile (Figure 4A). Thr131 donates a hydrogen bond to the ribose of the nicotinamide, positioning the C4 atom of the pyridine near the C6′ atom of the pyranose (Figure 4A). The most significant changes between the active and inhibited complexes are localized to the protein core between the active site and the hexamer-building interface. The feedback-inhibited structure shows that UDX binds to all six active sites in the broken hexamer (Figure 4B). The absence of the C5′-hydroxymethyl in UDX would be expected to create a void in the active site. Instead, Thr131 has moved ∼4 Å to pack against the C5′ atom of the xylose (Figures 4A and 5A,B). This inhibitor-specific induced-fit response prevents the cofactor from binding in a productive conformation; the α_N torsion angle of the nicotinamide ($O3-P_N-O5'_N-C5'_N$) rotates from −83° in the active conformation to 68° in the inhibited structure (Figures 4C and 5B). This conformation flips the nicotinamide into a solvent-exposed pocket where it is disordered, presumably because of poor packing.

Thr131 is part of a buried loop (residues 129−135, hereafter termed the Thr131 loop) connected to the α6 helix that straddles the rotation axes in the hexamer-building interface (Figure 3C). The repacking of the Thr131 loop causes the α6 helix to tilt by 10.6°, creating a surface that complements the rigid body rotations that form the broken-hexamer conformation (Figures 3C and 5A,B). The rotations bury ∼172 $Å^2$ more surface in each hexamer-building interface (776 ± 29 $Å^2$ per monomer), consistent with our observation that the UDX-bound hexamer is more stable than the high-symmetry complex (Figure 3D,E). Thus, the Thr131 loop is the molecular switch that allosterically changes the affinity of the hexamer-building interface in response to UDX binding. Rather than ratcheting the hexamer into the broken conformation, the weak high-symmetry complex likely dissociates, allowing the interface to repack into the more stable, low-symmetry conformation. There are no significant conformational differences between the exposed and

dx.doi.org/10.1021/bi2005637 |*Biochemistry* 2011, 50, 5780–5789

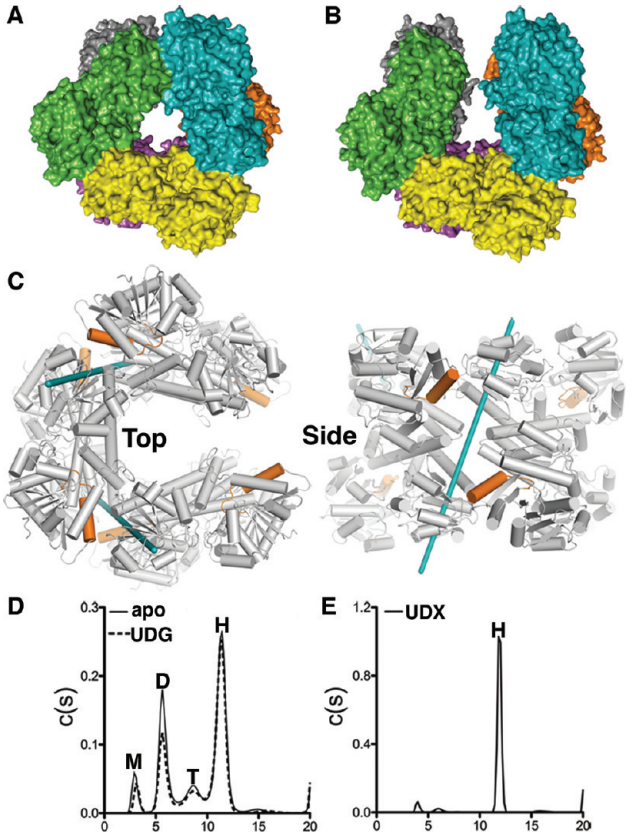

Figure 3. Feedback inhibition disrupts the oligomeric structure of hUGDH. (A) Solvent accessible surface of the high-symmetry conformation of the UDG-bound hUGDH hexamer (PDB entry 2Q3E) with each monomer colored differently. (B) Broken-hexamer form of UDX-inhibited hUGDH. (C) Top and side views of the broken hexamer with the rigid-body rotation axis depicted as teal rods passing through the hexamer-building interface. The Thr131 loop and α6 helix are colored orange (see the text). (D) Sedimentation velocity results of apo and UDG-bound hUGDH (solid and dashed lines, respectively). The $C(s)$ distribution reveals a heterogeneous mixture of sedimenting species [monomer (M, 3.1 S), dimer (D, 5.6 S), tetramer (T, 8.7 S), and hexamer (H, 11.5 S] (see Materials and Methods for details). (E) UDX stabilizes a hexameric species at 12.7 S.

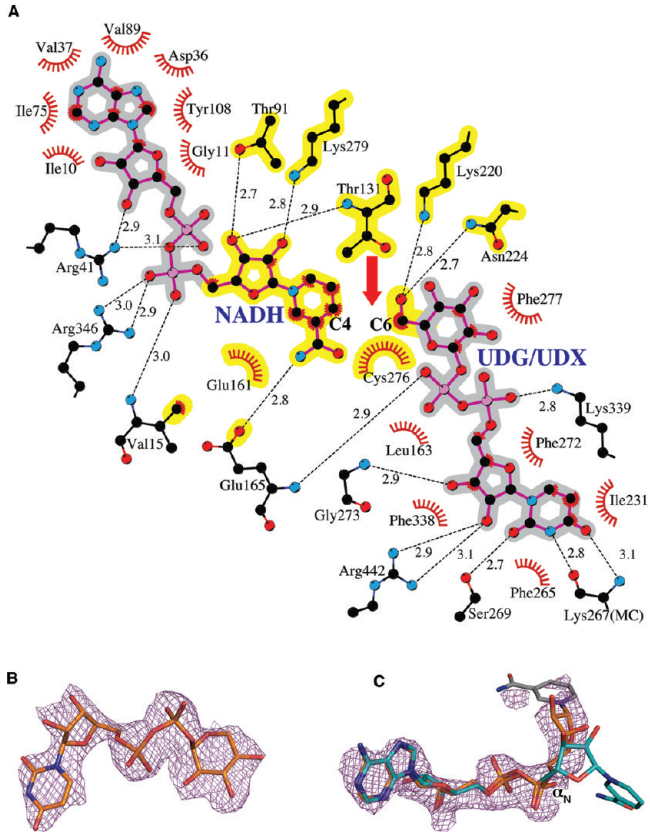

Figure 4. Substrate and inhibitor interactions in the active site of hUGDH. (A) This ligand plot depicts the hydrogen bonds (dashed lines) and packing interactions (red, feathered lines) between the substrate and cofactor in the active site of the enzyme. Interactions that are lost in the inhibited state are shaded yellow. The lack of a C5′-hydroxymethyl (labeled C6) induces the Thr131 to move into the active site (red arrow), blocking the nicotinamide ring from binding in a productive conformation. (B) $F_o - F_c$ difference map calculated following molecular replacement and an initial round of restrained refinement, but prior to modeling of the UDX molecule. The 2.5 Å resolution map is contoured at 3σ, and the ligand is from the final refined coordinates (PDB entry 3PTZ). (C) Same difference density as in panel B, but for the NAD^+ ligand (teal sticks), illustrating the disorder of the nicotinamide ring (gray sticks). The model for NADH bound in the high-symmetry hexamer (PDB entry 2Q3E) is superimposed to illustrate the rotation of the α_N torsion angle ($O3-P_N-O5'_N-C5'_N$).

buried hexamer-building interfaces in the broken-hexamer complex. It appears that the asymmetry of the complex is due to the repacking of the core, which produces a rotated interface incompatible with the formation of the high-symmetry hexamer.

Additional evidence linking the structure of the Thr131 loop to the stability of the complex comes from a comparison of the available structures. A superposition of the most structurally divergent monomers in the 2.5 and 3.1 Å resolution broken-hexamer complexes shows that the corresponding Cα atoms of residues 131−134 have an rmsd of 0.34 Å (Figure 5C). This variation in loop conformation is smaller than what would be expected from the coordinate error of the models (Luzzati coordinate errors of 0.31 and 0.61 Å for the 2.5 and 3.1 Å resolution structures, respectively). In contrast, the Thr131 loops in the high-symmetry hexamers show a much larger variation; a superposition of PDB entry 2Q3E onto PDB entries 3KHU, 2QG4, and 3ITK yields rmsd values of 0.89, 1.41, and 2.79 Å, respectively, for residues 131−134 (Figure 5D). The 3KHU and 2QG4 structures contain a reaction intermediate and the product UGA, respectively. The variability in the structure of the Thr131 loop in these structures likely reflects the conformational changes that would be expected to occur during the catalytic cycle. In the apo structure (PDB entry 3ITK), the Thr131 is mutated to alanine, and the loss of the threonine Cγ packing contributions to the protein core likely adds to the conformational differences (rmsd of 2.79 Å). These observations imply that the high-symmetry complexes have a more flexible hexamer-building interface, consistent with the sedimentation velocity studies showing a weaker complex in solution (Figure 3D,E).

Packing Defects Facilitate the Allosteric Transition of the Thr131 Loop. The induced-fit response of hUGDH to UDX requires a remarkable rearrangement of buried residues in the protein core (Figure 6 and Table 2). (i) The Cα atoms of the Thr131 loop translate through the core by ∼4 Å, shifting the register of the buried residues. (ii) The ϕ and ψ torsion angles of

dx.doi.org/10.1021/bi2005637 |*Biochemistry* 2011, 50, 5780–5789

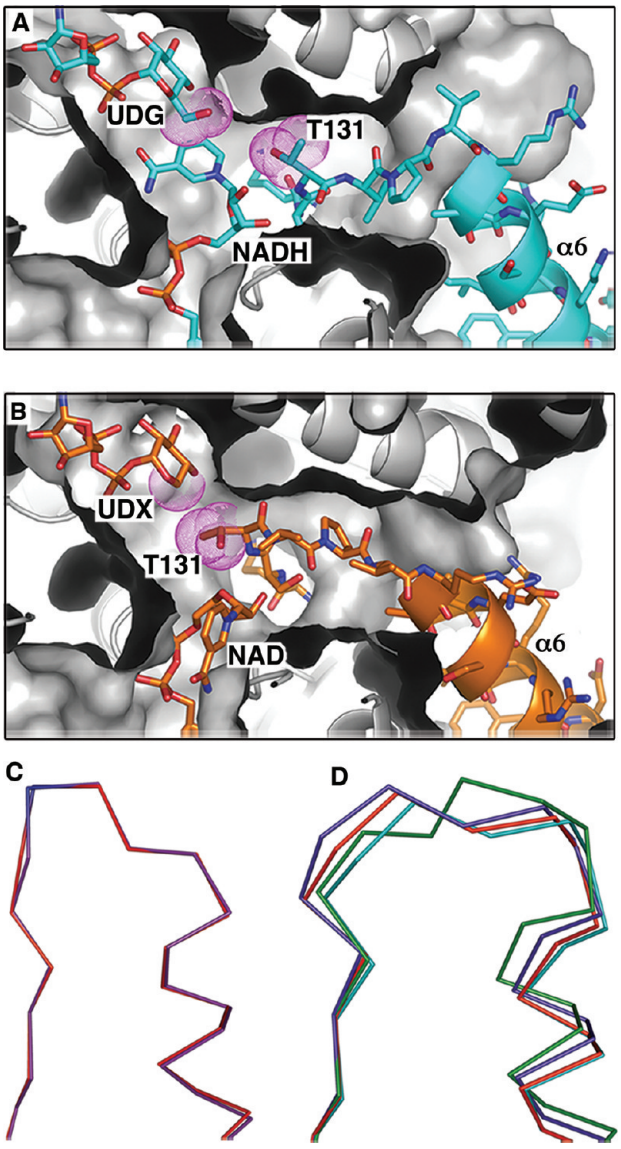

Figure 5. Thr131 loop that is key to the allosteric transition of hUGDH. (A) Cutaway of the molecular surface (gray) of the high-symmetry hexamer (PDB entry 2Q3E) depicting the "active" conformation of the Thr131 loop and α6 helix (teal sticks and cartoon). The buried Thr131 loop was excluded from the surface rendering, giving the appearance that it is in a tunnel passing through the protein core. UDG and NADH (sticks) are bound in the active site. The van der Waals radii (purple dots) are shown for the C5′-hydroxymethyl of UDG and the side chain of Thr131. (B) Same view as in panel A, but with UDX and NAD^+ bound in the broken hexamer. In response to the smaller van der Waals radii of the C5′ atom (purple dots) of UDX, the Thr131 loop (orange) has moved into the active site, causing the α6 helix to tilt in the hexamer-building interface. In this conformation, Thr131 prevents the nicotinamide from binding in a productive conformation. (C) Superimposed Cα traces showing the structural variation of the Thr131 loop from the broken-hexamer complexes: red for the 2.5 Å and purple for the 3.1 Å resolution complexes. (D) Superimposed Cα traces of the most structurally divergent Thr131 loops from the high-symmetry hexamers: teal (PDB entry 2Q3E), purple (PDB entry 3KHU), red (PDB entry 2QG4), and green (PDB entry 3ITK).

the Thr131 loop rotate, flipping Val132 and Pro133 by ∼180° around the axis of the main chain. (iii) Eight buried residues surrounding the loop change rotameric states. This repacking is facilitated by packing defects in the protein core. The structure of the high-symmetry hexamer (PDB entry 2Q3E) shows that five large packing defects (totaling 389 ± 10 $Å^3$) in the protein core are in contact with at least one residue in the Thr131 loop (Figure 7A). In the broken-hexamer conformation, the repacking of the core is reflected by changes in the volume (321 ± 32 $Å^3$), shape, and location of the packing defects (Figure 7B). Several water molecules are buried in the cavities, providing a means of satisfying the main chain hydrogen bonding requirements of the Thr131 loop in both conformations (Figure S1A,B of the Supporting Information). In the high-symmetry conformation, two of the main chain hydrogen bonds of the buried Thr131 loop are satisfied by one of the buried waters (Figure S1A of the Supporting Information). In the broken-hexamer conformation, the water structure rearranges so that two buried waters participate in three hydrogen bonds with the peptide backbone (Figure S1B of the Supporting Information).

How did hUGDH evolve the packing degeneracy needed to facilitate allosteric communication via the Thr131 loop? The equivalent Thr131 loop in the bacterial *Sp*UGDH structures adopts the same conformation seen in the dimers of the high-symmetry hUGDH hexamers (Figure 7C). Unlike the human enzyme, there is no induced-fit response upon UDX binding in *Sp*UGDH. The lack of a structural response is expected, because *S. pyogenes* does not make UDX and the activity of *Sp*UGDH is likely to be regulated by tyrosine phosphorylation, as in other bacteria.[34] A comparison of the protein cores surrounding the equivalent Thr131 loops in hUGDH and *Sp*UGDH reveals a dramatic structural divergence with respect to atomic packing density. The core surrounding the Thr131 loop in *Sp*UGDH buries a relatively small cavity (64 $Å^3$) (Figure 7C). In contrast, the evolution of the human enzyme has selected for six large-to-small cavity-forming substitutions surrounding the Thr131 loop (Figures 2C and 7D). These six substitutions represent a loss of hydrophobic residues and have left significant packing defects in the core. Engineering cavities using large-to-small substitutions has been shown to destabilize protein structure through a loss of packing interactions equivalent to ∼22 cal mol^{-1} $Å^{-3}$.[35,36] This implies that the cavities near the Thr131 loop in hUGDH represent a loss of ∼8 kcal mol^{-1} in packing interactions relative to those of *Sp*UGDH. Because the unfolded states of globular proteins are typically 4−15 kcal mol^{-1} less stable than the folded conformations,[37] the severe packing defects in hUGDH must have been favored during evolution. It is worth noting that the slightly smaller volume of the defects in the broken-hexamer conformation (321 ± 32 $Å^3$) implies a favorable gain of ∼1.6 kcal mol^{-1} in packing energy and may contribute to the observed stability of the broken-hexamer conformation.

We would expect the packing defects in the hUGDH structures to be reflected in the *B* factors of the Thr131 loop. Instead, the Thr131 loop is well-ordered in both the high- and low-symmetry hexamers and is comparable to other buried regions of the protein. Other factors likely contribute to the ordering of the Thr131 loop, specifically, (i) the hydrogen bonding and packing interactions between Thr131 and the ligands in the active site (Figures 4A and 5A,B) and (ii) the packing of the α6 helix in the hexamer-building interface (Figure 3C). Because the two conformations of the Thr131 loop are ordered, it is reasonable to assume that both conformations are energetically stable. This is consistent with the observed hysteresis in hUGDH activity;[18] if

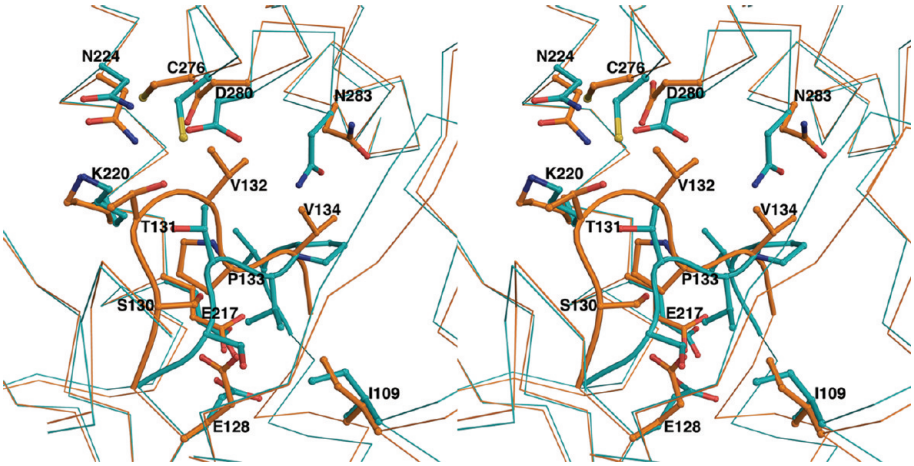

Figure 6. Allosteric transition requires the core to repack. Stereoview depicting the core packing degeneracy surrounding the Thr131 loop in the high-symmetry hexamer (teal) superimposed onto the broken hexamer (orange). The buried Thr131 loop undergoes a screwlike translation of ~4 Å, flipping Val132 and Pro133 by ~180° around the axis of the main chain. The eight buried residues that change rotameric states (Table 2) are shown.

Table 2. Changes in Buried Dihedrals That Contribute to the Packing Degeneracy

	Side Chain Rotameric Shifts			
residue	$\Delta\chi_1$[a]	$\Delta\chi_2$	$\Delta\chi_3$	$\Delta\chi_4$
Ile109	15°	101°		
Glu128	28°	91°	105°	
Glu217	11°	33°	2°	
Lys220	19°	8°	34°	105°
Asn224	23°	42°		
Cys276	117°			
Asp280	107°	69°		
Asn283	94°	74°		

	Main Chain Torsional Changes	
residue	$\Delta\phi$	$\Delta\psi$
Thr131	16°	157°
Val132	3°	63°
Pro133	37°	36°
Val134	57°	39°

[a] Dihedral angles are absolute differences between chain A in the hUGDH:UDG:NADH complex (PDB entry 2Q3E) and chain A in the hUGDH:UDX:NAD^+ complex.

the activation energy necessary to change the conformation of the Thr131 loop is relatively high, then a lag in progress curves could occur.

dCTP Deaminase Evolved Atypical Allostery by Selecting for Packing Defects. The bifunctional active−allosteric site in hUGDH represents an unusual form of heterotropic allostery. A similar feedback inhibition mechanism has also been described in an unrelated class of enzymes, the dCTP deaminases (dCTP-DA).[38,39] The dCTP-DA enzymes convert the nucleotide dCTP to dUTP, and the downstream metabolic product, dTTP, acts as a feedback inhibitor to regulate flux.[39,40] The feedback mechanism of dCTP-DA shares important features with that of hUGDH. (i) The substrate (dCTP) and inhibitor (dTTP) are structurally similar and compete for binding to the active site (Figure S2A,B of the Supporting Information), and (ii) the enzyme adopts a distinct induced-fit conformation in response to inhibitor binding (Figure 7E,F). As in hUGDH, a chemical difference between the substrate and the inhibitor (the C5-methyl of dTTP) induces a buried loop (the A115 loop) to rearrange and change the conformation of the dCTP-DA complex (Figure 7E,F and Figure S2C,D of the Supporting Information). Our analysis shows that this conformational change is facilitated by large packing defects in the core and subunit interfaces (Figure 7E,F and Figure S2C,D of the Supporting Information). The dCTP-DAs are closely related to the nonallosteric dUTPases.[39,41] In fact, the active sites in the dCTP-DAs from *M. tuberculosis* and *Methanococcus jannaschii* conserve both the dUTPase catalytic residues and activity.[38,41] By comparing the dUTPases with the dCTP-DAs, we observe that the latter enzymes have selected for large packing defects during evolution to accommodate the inhibitor-specific induced-fit response (Figure 7E−G and Figure S2C−E of the Supporting Information).

Role of Packing Defects in the Evolution of Allostery and Induced Fit. Allostery occurs when an effector binding to one site of a protein changes the affinity of another, distant binding site. In the case of hUGDH, UDX binding to the active site increases the affinity between dimers to form the broken hexamer (Figure 3E). But how does an allosteric interaction network evolve? The core of a natively folded protein is a relatively rigid structure, with atoms typically packed at densities approaching or surpassing that of closely packed spheres.[19] Previous studies have shown that engineering a packing defect into a nonallosteric enzyme can be sufficient to induce substrate (or homotropic) cooperativity (Figure 8A).[42−44] Packing defects add flexibility to the protein core;[45] thus, introducing a defect can produce a more conformationally diverse ensemble of structures.[46] Homotropic allostery will occur only if a subset of the resulting ensemble adopts a conformation favoring the formation of the Michaelis complex.[46] Substrate binding stabilizes protein structure and reduces flexibility.[47] In an oligomeric complex, the substrate-induced stabilization of one subunit would be reflected in an ordering of the interface (Figure 8A). Thus, homotropic cooperativity is due to symmetry; ligand binding to one subunit would restrain the flexibility of an adjacent subunit to conformations resembling the Michaelis complex, increasing the affinity for the substrate.

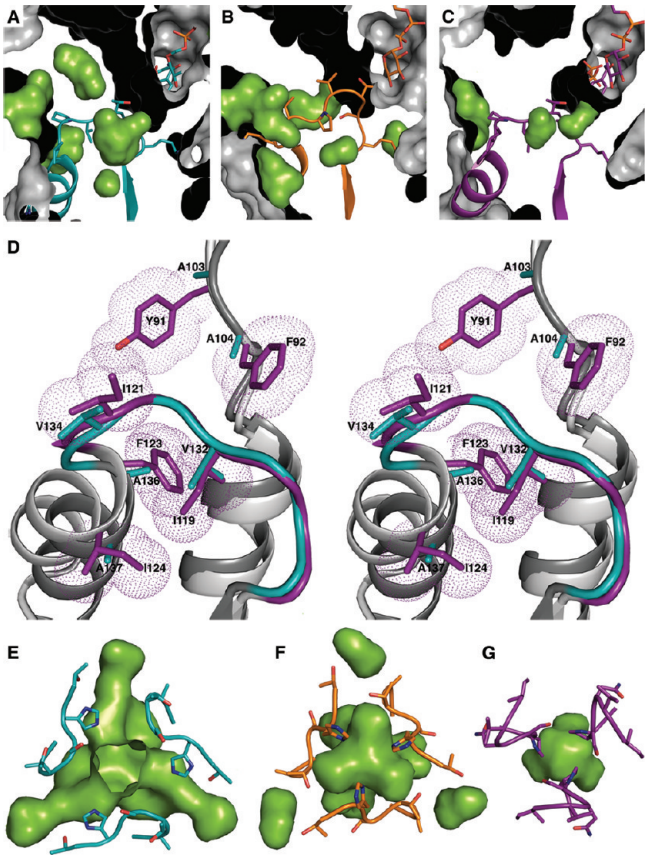

Figure 7. Packing defects facilitate alternate core arrangements in hUGDH and dCTP deaminase. (A) Cutaway of the molecular surface of the high-symmetry hUGDH structure (PDB entry 2Q3E) showing the packing defects in the core (cavities and deep pockets, green surface) surrounding the buried Thr131 loop (teal). UDG (teal, sticks) is depicted in the active site (top right). Cavity surfaces were calculated using a 1.4 Å probe. (B) Same orientation as in panel A, depicting the changes in the packing defects that occur in the UDX-bound broken-hexamer conformation. (C) Same orientation as in panel A, illustrating the smaller packing defects surrounding the equivalent Thr131 loop in the *Sp*UGDH:UDX complex (PDB entry 1DLI). Because of the smaller cavity size, the surfaces were generated using a 1.3 Å probe radius for the sake of clarity. (D) Stereoview illustrating the six large-to-small substitutions that have occurred during the evolution of packing degeneracy. hUGDH (teal, PDB entry 2Q3E) is superimposed onto the *Sp*UGDH:UDX complex (purple, PDB entry 1DLI) (Figure 2C). Purple dots depict the van der Waals radii of the large hydrophobic residues in the bacterial structure. (E) Cavities (green surfaces) in the interface and core of allosteric *Mycobacterium tuberculosis* dCTP-DA (PDB entry 2QLP, teal) shown looking down the 3-fold axis of the trimeric enzyme. The A115 loops in the active site of the three subunits are shown. (F) Same view as in panel E, except showing the changes in packing defects in inhibited *M. tuberculosis* dCTP-DA (PDB entry 2QXX, orange). (G) Same view as in panel E, but depicting the smaller cavities in the homologous, nonallosteric *M. tuberculosis* dUTPase (PDB entry 1SLH, purple). All cavity surfaces were generated using a 1.4 Å probe.

In the case of classic heterotropic allostery, the effector and the substrate are chemically distinct molecules that bind to separate sites (Figure 8B). In this way, a metabolic end product can control its own synthesis by binding to and inhibiting an earlier enzyme in the same biochemical pathway. Still, the evolution of a specialized allosteric binding site for a heterotropic effector

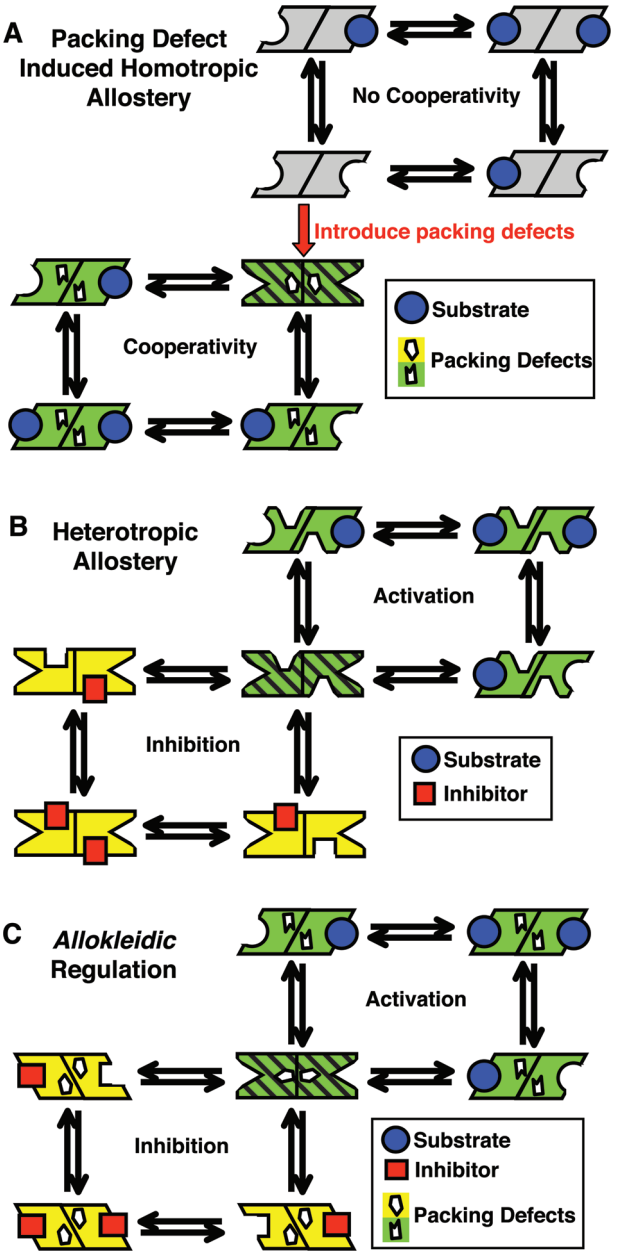

Figure 8. Allosteric regulation in enzymes. (A) Cartoon of a dimeric enzyme illustrating how homotropic allostery can be induced by packing defects. In the absence of packing defects (gray shading), the conformational state of the dimer favors the active, high-substrate affinity state (right-leaning diagonal). Packing defects (white cutouts) add flexibility to the complex, producing a conformational ensemble (black hatching) with different substrate affinities (triangular binding site). Substrate binding (blue circle) to one subunit selects for the high-substrate affinity conformation (green shading), explaining the observed homotropic cooperativity. (B) Similar cartoon depicting classic heterotropic feedback inhibition in enzymes. In the absence of the substrate, the enzyme is represented as a conformational ensemble (black hatching) with different affinities for the substrate (blue circle) and inhibitor (red square). Substrate binding shifts the ensemble to the high-substrate affinity state (green). Inhibitor binding selects for the low-substrate affinity states (yellow). (C) *Allokleidic* regulation in enzymes. Because of packing defects (white cutouts) selected during evolution, the *allokleidic* enzyme is represented as a conformational ensemble (black hatching) with varying affinities for the substrate (blue circle) and inhibitor (red square). Substrate or inhibitor binding acts as described above, the exception being that both ligands compete for the same bifunctional *allokleidic* site.

dx.doi.org/10.1021/bi2005637 |*Biochemistry* 2011, 50, 5780–5789

would appear to be a complex process. In contrast, both hUGDH and dCTP-DA have evolved an atypical form of heterotropic allostery based on a single, bifunctional binding site: the active site can support catalysis or regulate enzyme activity in response to the chemical identity of the bound ligand (Figure 5A,B). When the substrate binds, the Thr131 loop is positioned to support catalysis. When the inhibitor binds, the Thr131 loop conforms to the chemical differences and switches the enzyme into an inactive state. Because the Thr131 loop directly connects the hexamer-building interface to the active site, it is possible to allosterically transfer information between adjacent molecules (Figure 5A,B). To explain specificity, Emil Fischer proposed that a substrate molecule fits into the active site much like a key into a lock. In keeping with the original nomenclature of Monod,[48] and with deference to Fischer's model, we call this dual specificity active site an *allokleidic* (*allos* "other" and *kleidi* "key") site. Because most downstream metabolites are structurally similar to the substrates earlier in the pathway, the selection of an *allokleidic* mechanism offers an evolutionary advantage; relatively few adaptations to the active site would be required to bind a structurally similar effector. Our observation that two unrelated metabolic checkpoint enzymes (hUGDH and dCTP-DA) have converged to similar feedback mechanisms is good evidence that the evolution of an *allokleidic* active site offers a robust alternative to the selection for a separate allosteric site.

The *allokleidic* mechanism we have described is based on alternate core packing arrangements as part of an inhibitor-specific induced-fit response. Still, the steric complementarity constraints of a densely packed core[19] make it difficult to envision alternate stable packing arrangements for buried amino acids (Figure 6). How did hUGDH and dCTP-DA evolve core packing degeneracy? The nonallosteric homologues of both families contain relatively small packing defects in the same regions of the protein core where the allosteric members evolved *allokleidic* switches (Figure 7 and Figure S2 of the Supporting Information). Residues near existing packing defects are known to exhibit higher rates of sequence divergence relative to those of densely packed residues.[49] Together, these observations imply that the ancestral proteins in the UGDH and dCTP-DA families acquired the packing defects prior to the divergence of the nonallosteric and allosteric enzymes. Afterward, the allosteric members of the two families followed a relatively simple evolutionary strategy, the selection for cavities near existing packing defects. Packing defects are known to contribute to promiscuous binding[50] and conformational flexibility,[45] two valuable adaptive traits in the evolution of induced fit and allostery. Thus, the UGDH and dCTP-DA examples support our hypothesis that packing defects represent hot spots for the evolution of both allosteric networks and induced-fit mechanisms.

■ ASSOCIATED CONTENT

Ⓢ Supporting Information. Buried water molecules that hydrogen bond to the main chain of the Thr131 loop in the active and inhibited hUGDH complexes (Figure S1) and evolution of packing degeneracy in the *Escherichia coli* dCTP-DA family (Figure S2). This material is available free of charge via the Internet at http://pubs.acs.org.

Accession Codes

The atomic coordinates and structure factors have been deposited in the Protein Data Bank as entries 3PTZ and 3PRJ.

■ AUTHOR INFORMATION

Corresponding Author

*Phone: (706) 583-0304. Fax: (706) 542-1738. E-mail: zac@bmb.uga.edu.

Funding Sources

Funding from the University of Georgia Research Alliance and American Cancer Society Grant RSG0918401DMC to Z.A.W. is gratefully acknowledged.

■ ACKNOWLEDGMENT

We thank Walt Baase (University of Oregon) for helpful discussions, William Lanzilotta (University of Georgia), and the SER-CAT beamline personnel (Advanced Photon Source, Argonne National Laboratory, Argonne, IL) for help with data collection.

■ REFERENCES

(1) Belting, M., Borsig, L., Fuster, M. M., Brown, J. R., Persson, L., Fransson, L. A., and Esko, J. D. (2002) Tumor attenuation by combined heparan sulfate and polyamine depletion. *Proc. Natl. Acad. Sci. U.S.A. 99*, 371–376.

(2) Sanderson, R. D., Yang, Y., Kelly, T., MacLeod, V., Dai, Y., and Theus, A. (2005) Enzymatic remodeling of heparan sulfate proteoglycans within the tumor microenvironment: Growth regulation and the prospect of new cancer therapies. *J. Cell. Biochem. 96*, 897–905.

(3) Fuster, M. M., and Esko, J. D. (2005) The sweet and sour of cancer: Glycans as novel therapeutic targets. *Nat. Rev. Cancer 5*, 526–542.

(4) Itano, N., and Kimata, K. (2008) Altered hyaluronan biosynthesis in cancer progression. *Semin. Cancer Biol. 18*, 268–274.

(5) Stern, R. (2008) Association between cancer and "acid mucopolysaccharides": An old concept comes of age, finally. *Semin. Cancer Biol. 18*, 238–243.

(6) Cummings, J., Boyd, G., Ethell, B. T., Macpherson, J. S., Burchell, B., Smyth, J. F., and Jodrell, D. I. (2002) Enhanced clearance of topoisomerase I inhibitors from human colon cancer cells by glucuronidation. *Biochem. Pharmacol. 63*, 607–613.

(7) Cummings, J., Ethell, B. T., Jardine, L., Boyd, G., Macpherson, J. S., Burchell, B., Smyth, J. F., and Jodrell, D. I. (2003) Glucuronidation as a mechanism of intrinsic drug resistance in human colon cancer: Reversal of resistance by food additives. *Cancer Res. 63*, 8443–8450.

(8) Cummings, J., Ethell, B. T., Jardine, L., and Burchell, B. (2006) Glucuronidation of SN-38 and NU/ICRF 505 in human colon cancer and adjacent normal colon. *Anticancer Res. 26*, 2189–2196.

(9) Cummings, J., Zelcer, N., Allen, J. D., Yao, D., Boyd, G., Maliepaard, M., Friedberg, T. H., Smyth, J. F., and Jodrell, D. I. (2004) Glucuronidation as a mechanism of intrinsic drug resistance in colon cancer cells: Contribution of drug transport proteins. *Biochem. Pharmacol. 67*, 31–39.

(10) Cecchin, E., Innocenti, F., D'Andrea, M., Corona, G., De Mattia, E., Biason, P., Buonadonna, A., and Toffoli, G. (2009) Predictive role of the UGT1A1, UGT1A7, and UGT1A9 genetic variants and their haplotypes on the outcome of metastatic colorectal cancer patients treated with fluorouracil, leucovorin, and irinotecan. *J. Clin. Oncol. 27*, 2457–2465.

(11) Oguri, T., Takahashi, T., Miyazaki, M., Isobe, T., Kohno, N., Mackenzie, P. I., and Fujiwara, Y. (2004) UGT1A10 is responsible for SN-38 glucuronidation and its expression in human lung cancers. *Anticancer Res. 24*, 2893–2896.

(12) Takahashi, T., Fujiwara, Y., Yamakido, M., Katoh, O., Watanabe, H., and Mackenzie, P. I. (1997) The role of glucuronidation in 7-ethyl-10-hydroxycamptothecin resistance in vitro. *Jpn. J. Cancer Res. 88*, 1211–1217.

(13) Neufeld, E. F., and Hall, C. W. (1965) Inhibition of UDP-D-Glucose Dehydrogenase by UDP-D-Xylose: A Possible Regulatory Mechanism. *Biochem. Biophys. Res. Commun. 19*, 456–461.

(14) Bakker, H., Oka, T., Ashikov, A., Yadav, A., Berger, M., Rana, N. A., Bai, X., Jigami, Y., Haltiwanger, R. S., Esko, J. D., and Gerardy-Schahn, R. (2009) Functional UDP-xylose transport across the endoplasmic reticulum/Golgi membrane in a Chinese hamster ovary cell mutant defective in UDP-xylose synthase. *J. Biol. Chem. 284*, 2576–2583.

(15) Gainey, P. A., and Phelps, C. F. (1975) Interactions of urdine diphosphate glucose dehydrogenase with the inhibitor urdine diphosphate xylose. *Biochem. J. 145*, 129–134.

(16) Ainslie, G. R., Jr., Shill, J. P., and Neet, K. E. (1972) Transients and cooperativity. A slow transition model for relating transients and cooperative kinetics of enzymes. *J. Biol. Chem. 247*, 7088–7096.

(17) Frieden, C. (1979) Slow transitions and hysteretic behavior in enzymes. *Annu. Rev. Biochem. 48*, 471–489.

(18) Dickinson, F. M. (1988) Studies on the unusual behaviour of bovine liver UDP-glucose dehydrogenase in assays at acid and neutral pH and on the presence of tightly bound nucleotide material in purified preparations of this enzyme. *Biochem. J. 255*, 775–780.

(19) Richards, F. M. (1977) Areas, volumes, packing and protein structure. *Annu. Rev. Biophys. Bioeng. 6*, 151–176.

(20) van den Berg, S., Lofdahl, P. A., Hard, T., and Berglund, H. (2006) Improved solubility of TEV protease by directed evolution. *J. Biotechnol. 121*, 291–298.

(21) Kabsch, W. (2010) Xds. *Acta Crystallogr. D66*, 125–132.

(22) McCoy, A. J., Grosse-Kunstleve, R. W., Adams, P. D., Winn, M. D., Storoni, L. C., and Read, R. J. (2007) Phaser crystallographic software. *J. Appl. Crystallogr. 40*, 658–674.

(23) Emsley, P., and Cowtan, K. (2004) Coot: Model-building tools for molecular graphics. *Acta Crystallogr. D60*, 2126–2132.

(24) Vagin, A. A., Steiner, R. A., Lebedev, A. A., Potterton, L., McNicholas, S., Long, F., and Murshudov, G. N. (2004) REFMAC5 dictionary: Organization of prior chemical knowledge and guidelines for its use. *Acta Crystallogr. D60*, 2184–2195.

(25) Hayward, S., and Berendsen, H. J. (1998) Systematic analysis of domain motions in proteins from conformational change: New results on citrate synthase and T4 lysozyme. *Proteins 30*, 144–154.

(26) Dundas, J., Ouyang, Z., Tseng, J., Binkowski, A., Turpaz, Y., and Liang, J. (2006) CASTp: Computed atlas of surface topography of proteins with structural and topographical mapping of functionally annotated residues. *Nucleic Acids Res. 34*, W116–W118.

(27) Laue, T. M., Shah, B. D., Ridgeway, T. M., and Pelletier, S. L. (1992) Computer-aided interpretation of analytical sedimentation data for proteins. In *Analytical ultracentrifugation in biochemistry and polymer science* (Harding, S. E., Rowe, A. J., and Horton, J. C., Eds.) pp 90−125, The Royal Society of Chemistry, Cambridge, U.K.

(28) Brown, P. H., and Schuck, P. (2006) Macromolecular size-and-shape distributions by sedimentation velocity analytical ultracentrifugation. *Biophys. J. 90*, 4651–4661.

(29) Campbell, R. E., Mosimann, S. C., van De Rijn, I., Tanner, M. E., and Strynadka, N. C. (2000) The first structure of UDP-glucose dehydrogenase reveals the catalytic residues necessary for the two-fold oxidation. *Biochemistry 39*, 7012–7023.

(30) Sommer, B. J., Barycki, J. J., and Simpson, M. A. (2004) Characterization of human UDP-glucose dehydrogenase. CYS-276 is required for the second of two successive oxidations. *J. Biol. Chem. 279*, 23590–23596.

(31) Huh, J. W., Yoon, H. Y., Lee, H. J., Choi, W. B., Yang, S. J., and Cho, S. W. (2004) Importance of Gly-13 for the coenzyme binding of human UDP-glucose dehydrogenase. *J. Biol. Chem. 279*, 37491–37498.

(32) Zhang, X. J., Wozniak, J. A., and Matthews, B. W. (1995) Protein flexibility and adaptability seen in 25 crystal forms of T4 lysozyme. *J. Mol. Biol. 250*, 527–552.

(33) Dickerson, R. E., Goodsell, D. S., and Neidle, S. (1994) The tyranny of the lattice. *Proc. Natl. Acad. Sci. U.S.A. 91*, 3579–3583.

(34) Lacour, S., Bechet, E., Cozzone, A. J., Mijakovic, I., and Grangeasse, C. (2008) Tyrosine phosphorylation of the UDP-glucose dehydrogenase of *Escherichia coli* is at the crossroads of colanic acid synthesis and polymyxin resistance. *PLoS One 3*, e3053.

(35) Eriksson, A. E., Baase, W. A., Zhang, X. J., Heinz, D. W., Blaber, M., Baldwin, E. P., and Matthews, B. W. (1992) Response of a protein structure to cavity-creating mutations and its relation to the hydrophobic effect. *Science 255*, 178–183.

(36) Joh, N. H., Oberai, A., Yang, D., Whitelegge, J. P., and Bowie, J. U. (2009) Similar energetic contributions of packing in the core of membrane and water-soluble proteins. *J. Am. Chem. Soc. 131*, 10846–10847.

(37) Kumar, M. D., and Gromiha, M. M. (2006) PINT: Protein-protein Interactions Thermodynamic Database. *Nucleic Acids Res. 34*, D195–D198.

(38) Helt, S. S., Thymark, M., Harris, P., Aagaard, C., Dietrich, J., Larsen, S., and Willemoes, M. (2008) Mechanism of dTTP inhibition of the bifunctional dCTP deaminase:dUTPase encoded by *Mycobacterium tuberculosis*. *J. Mol. Biol. 376*, 554–569.

(39) Johansson, E., Thymark, M., Bynck, J. H., Fano, M., Larsen, S., and Willemoes, M. (2007) Regulation of dCTP deaminase from *Escherichia coli* by nonallosteric dTTP binding to an inactive form of the enzyme. *FEBS J. 274*, 4188–4198.

(40) Beck, C. F., Eisenhardt, A. R., and Neuhard, J. (1975) Deoxycytidine triphosphate deaminase of *Salmonella typhimurium*. Purification and characterization. *J. Biol. Chem. 250*, 609–616.

(41) Johansson, E., Bjornberg, O., Nyman, P. O., and Larsen, S. (2003) Structure of the bifunctional dCTP deaminase-dUTPase from *Methanocaldococcus jannaschii* and its relation to other homotrimeric dUTPases. *J. Biol. Chem. 278*, 27916–27922.

(42) Kolodziej, A. F., Tan, T., and Koshland, D. E., Jr. (1996) Producing positive, negative, and no cooperativity by mutations at a single residue located at the subunit interface in the aspartate receptor of *Salmonella typhimurium*. *Biochemistry 35*, 14782–14792.

(43) Scrutton, N. S., Deonarain, M. P., Berry, A., and Perham, R. N. (1992) Cooperativity induced by a single mutation at the subunit interface of a dimeric enzyme: Glutathione reductase. *Science 258*, 1140–1143.

(44) Kuo, L. C., Zambidis, I., and Caron, C. (1989) Triggering of allostery in an enzyme by a point mutation: Ornithine transcarbamoylase. *Science 245*, 522–524.

(45) Bahar, I., Atilgan, A. R., and Erman, B. (1997) Direct evaluation of thermal fluctuations in proteins using a single-parameter harmonic potential. *Folding Des. 2*, 173–181.

(46) Gunasekaran, K., Ma, B., and Nussinov, R. (2004) Is allostery an intrinsic property of all dynamic proteins? *Proteins 57*, 433–443.

(47) Ma, B., Kumar, S., Tsai, C. J., and Nussinov, R. (1999) Folding funnels and binding mechanisms. *Protein Eng. 12*, 713–720.

(48) Monod, J., Changeux, J. P., and Jacob, F. (1963) Allosteric proteins and cellular control systems. *J. Mol. Biol. 6*, 306–329.

(49) Liao, H., Yeh, W., Chiang, D., Jernigan, R. L., and Lustig, B. (2005) Protein sequence entropy is closely related to packing density and hydrophobicity. *Protein Eng., Des. Sel. 18*, 59–64.

(50) Tokuriki, N., and Tawfik, D. S. (2009) Protein dynamism and evolvability. *Science 324*, 203–207.